Numerical studies of confined states in rotated bilayers of graphene

G. Trambly de Laissardière,[1,*] D. Mayou,[2,†] and L. Magaud[2,‡]

[1]*Laboratoire de Physique Théorique et Modélisation, Université de Cergy-Pontoise - CNRS, F-95302 Cergy-Pontoise, France*

[2]*Institut Néel, CNRS - Université Joseph Fourier, F-38042 Grenoble, France*

(Received 27 March 2012; revised manuscript received 31 July 2012; published 7 September 2012)

Rotated graphene multilayers form a new class of graphene-related systems with electronic properties that drastically depend on the rotation angles. It has been shown that bilayers behave like two isolated graphene planes for large rotation angles. For smaller angles, states in the Dirac cones belonging to the two layers interact resulting in the appearance of two Van Hove singularities. States become localized as the rotation angle decreases and the two Van Hove singularities merge into one peak at the Dirac energy. Here we go further and consider bilayers with very small rotation angles. In this case, well-defined regions of AA stacking exist in the bilayer supercell and we show that states are confined in these regions for energies in the $[-\gamma_t, +\gamma_t]$ range with γ_t the interplane mean interaction. As a consequence, the local densities of states show discrete peaks for energies different from the Dirac energy.

DOI: 10.1103/PhysRevB.86.125413 PACS number(s): 73.20.At, 73.20.−r, 73.21.Ac, 61.48.Gh

I. INTRODUCTION

Graphene exceptional electronic properties are predicted for an isolated layer of C atoms arranged on a pristine honeycomb lattice.[1,2] Stacking several layers on top of each other may affect the original electronic structure. Indeed AB or Bernal stacking (such as what is found in graphite) destroys both the linear dispersion and the chirality properties even in a bilayer.[3–8] Many experimental realizations of graphene lead to the formation of multilayers (on SiC[6–14] but also on metal surfaces such as Ni[15] and in exfoliated flakes[16]) where interactions between successive layers play a crucial role. While on the Si face of SiC, multilayers have an AB stacking and do not show graphene properties,[5–8] on the C face, multilayers have been shown to present graphene-like properties even when they involve a large number of C planes. ARPES,[11–13] STM,[17] transport,[18] and optical transitions[19] indeed show properties characteristic of a linear graphene-like dispersion. These multilayers are rotated with respect to each other and the rotations show up as moiré patterns on STM images.[14,20,21] This apparent controversy—thick multilayers exhibiting graphene properties—was partially solved recently when different theoretical approaches[14,22–31] showed that rotated multilayers are decoupled, at least for large rotation angles. Going further, theory predicts the existence of three domains that in fact correspond to two regimes: For large rotation angles, $\theta > 15^\circ$, the layers are decoupled and behave as a collection of isolated graphene layers. For intermediate angles, $2^\circ < \theta < 15^\circ$, the dispersion remains linear but the velocity is renormalized. For these large and intermediate angles, Dirac cones persist and the interaction between rotated layers is a perturbation. What happens at the smallest values of θ is more puzzling. As already shown by different theoretical groups, for the lowest θ, flat bands appear and result in electronic localization.

From the experimental point of view, while some experiments with graphene on SiC show none of the effects predicted by theory (no renormalization or Van Hove singularities),[13] others[32] do find them. Furthermore, Landau level (LL) scanning tunneling spectroscopy (STS) gave results in close agreement with theory and the three domains were observed for CVD graphene grown on Ni.[15]

Here we go further and show that in the very small angle regime, confinement occurs and states become confined in the AA (all atoms on top of each other) region. Furthermore, confinement effects lead to the formation of sharp peaks in the local density of states in an energy window that is fixed by the interplane mean interaction. Thus, this apparently simple system—a graphene bilayer—presents a complex behavior ranging from ballistic to confined electrons when the rotation angle is changed.

Tackling very small rotation angles—smaller than 1°—means handling very large cells that involve a huge number of atoms—more than 60 000. This cannot be done from *ab initio* calculations and we developed a tight-binding scheme[31] using only p_z orbitals to do so. Rotated multilayers are described in Sec. II, the method used is outlined in Sec. III and described in more details in the Appendix. Section IV gives the variation of the Van Hove singularity position with the rotation angle, and Secs. V and VI describe the electronic structure of graphene rotated bilayers in the case of very small rotation angles.

II. ROTATIONALLY STACKED COMMENSURATE BILAYERS

In the following we consider two graphene layers rotated in the plane by an angle θ. We start from an AA bilayer and choose the rotation origin O at an atomic site. Since we want to perform *ab initio* and tight-binding calculations, we need a periodic system. A commensurate structure can be defined if the rotation changes a lattice vector $\overrightarrow{OB}(m,n)$ to $\overrightarrow{OB'}(n,m)$ with n, m the coordinates with respect to the basis vectors $\vec{a}_1$ $(\sqrt{3}/2, -1/2)$ and $\vec{a}_2$ $(\sqrt{3}/2, 1/2)$. The rotation angle is then defined as follows:

$$\cos\theta = \frac{n^2 + 4nm + m^2}{2(n^2 + nm + m^2)}, \tag{1}$$

and the commensurate cell vectors correspond to

$$\vec{t} = \overrightarrow{OB'} = n\vec{a}_1 + m\vec{a}_2, \quad \vec{t'} = -m\vec{a}_1 + (n+m)\vec{a}_2. \tag{2}$$

The commensurate unit cell contains $N = 4(n^2 + nm + m^2)$ atoms. As we have already shown,[31] the rotation angle

is a good parameter to describe the system but the number of atoms is not since cells of equivalent size can be found for different angles. Indeed, large cells can be obtained for $\theta \sim 0$—large n and m and small $|m-n|$—but also for large angles $\theta \sim 30°$—then $|m-n|$ is large .[33] A good way to name the rotated layers is to give the (n,m) couple defined above, which is what we use in the present paper. $\theta = 60°$ is the perfect AB stacking. θ close to 60° is obtained for $n = 1$ ($m = 1$) and large m (n); it is equivalent in our calculations to $\theta \sim 0°$.

III. METHODS

Our approach combines *ab initio* and tight-binding calculations. A first-principles approach can tackle cells with up to ∼1000 atoms. The tight-binding (TB) scheme allows electronic structure calculations by diagonalization in reciprocal space for crystal structures containing up to 59 644 atoms in a unit cell—corresponding to $\theta = 0.469°$ and the (70,71) bilayer. By the using recursion technique in real space, very large structures up to several millions—3 006 004 for the (500,501) with $\theta = 0.067°$—of atoms are studied. The tight-binding scheme is described in Ref. 31 and the Appendix; it is restricted to p_z orbitals. It was developed from *ab initio* calculations and it gives a good description of the rotated bilayers, for small angles as well as large ones but also for trilayers, graphene, and graphite. The TB parameters were fitted to reproduce the velocity of monolayer graphene and the interlayer mean interaction $\gamma_t = 0.34$ eV (see Appendix). Flat layers were used. We performed an *ab initio* calculation for the (6,7) bilayer allowing all the atoms to relax and found only minor changes: The layer corrugation is small and the effect on the band structure is very small.[34] Velocities are calculated from the slope of the dispersions at the Dirac point along ΓK.

IV. VAN HOVE SINGULARITIES

The rotated bilayer has already been the subject of many theoretical developments either analytical or numerical.[14,22–31] The main results are only briefly recalled in the following since we want to focus on the very small rotation case and the confinement effect that results. These theoretical predictions are in very good agreement with scanning tunneling spectroscopy experiments on CVD graphene grown on nickel.[15] Properties are symmetric with respect to $\theta = 30°$: In our calculations, the behavior is the same for angles decreasing to 0° or increasing to 60°.

For large angles, $\theta > 15°$, the rotated bilayer behaves like two isolated graphene layers. For intermediate angles, $2° < \theta < 15°$, the dispersion remains linear but the velocity is strongly renormalized. In this regime, one important feature is the appearance of Van Hove singularities on both sides of the Dirac energy. In the following, we consider that layer 2 is rotated by an angle θ with respect to layer 1. The layer 2 Brillouin zone is then rotated by the same θ with respect to the layer 1 Brillouin zone. The closest Dirac cones belonging to layer 1 and 2 intersect at a point P which is at mid-distance between the K_1 and K_2 points of the 1×1 Brillouin zones [see Fig. 1(a)]. P is backfolded to point M of the supercell Brillouin zone. Interaction of the states with similar energies opens two gaps at the saddle point M [Fig. 1(b)]. Flat bands have a drastic

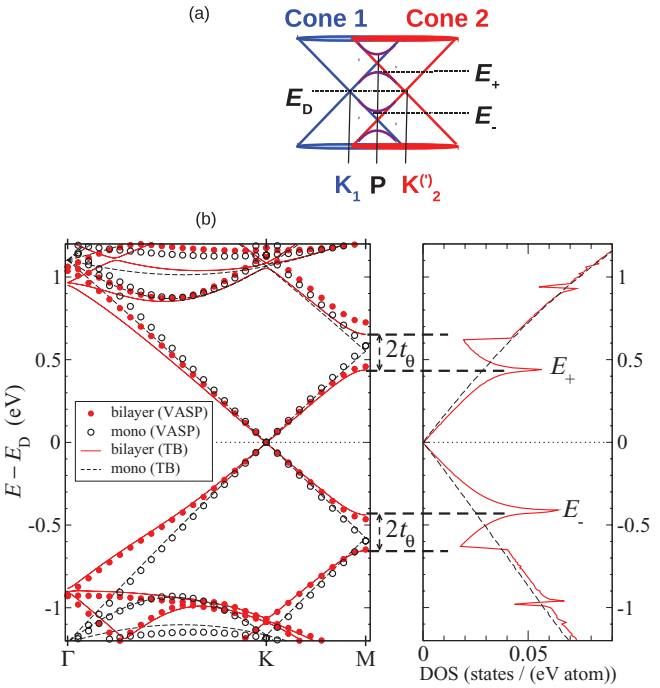

FIG. 1. (Color online) Van Hove singularities of a (4,5) bilayer, $\theta = 7.34°$. (a) Schematic drawing. (b) (4,5) band structure and total DOS.

effect on the electronic structure of two-dimensional systems and appear as Van Hove singularities on each side of the Dirac energy [Fig. 1(b)]. In fact, each gap creates two Van Hove singularities: Singularities closest to the Dirac point appear as peaks E_+ and E_- in Fig. 1(b); they are followed by a dip and a sharp increase of the DOS that corresponds to the flat bands on the other side of the gaps. The gap width and then the energy difference between the steep increase in the DOS and the peak are equal to $2t_\theta$ with t_θ the mean interaction between states related to the two layers at the intersection between the Dirac cones, as defined by Ref. 23.

In Fig. 2, the energies E_+ and E_- of the closest peaks to the Dirac energy are plotted versus θ. For intermediated angle values, $2° < \theta < 15°$, E_+ and E_- are linear with respect to θ.

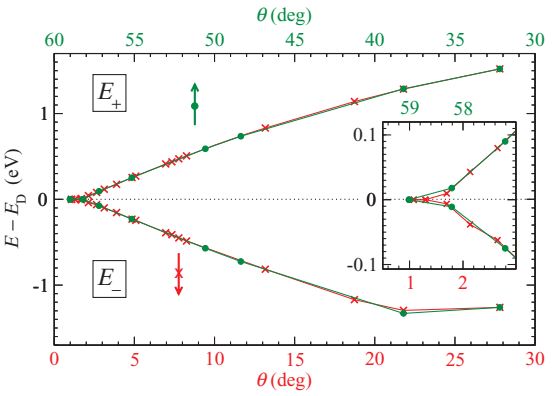

FIG. 2. (Color online) Energies of the Van Hove singularities (the two peaks closest to E_D) in (n,m) bilayers versus θ. Lines are guides for the eyes.

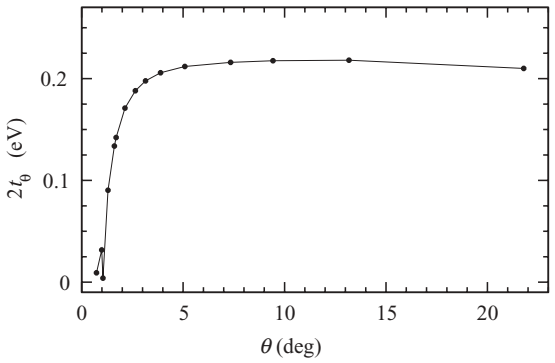

FIG. 3. Gap at P (point M of the supercell) as a function of θ. Line is a guide for the eyes.

As the rotation angle decreases, the intersections of the two Dirac cones belonging to the two graphene layers come closer to the Dirac energy (Fig. 1). The intersection point P is at mid-distance between K_1 and K_2. The K_1K_2 distance decreases linearly with θ. Since in this regime the dispersion is linear and the gap at P is roughly constant (Fig. 3), the position of the Van Hove singularities then varies linearly with θ. For small angle values, $\theta \sim 2^\circ$, E_+ and E_- merge and form a sharp peak at the Dirac energy E_D.

As shown in our previous article,[31] this sharp peak corresponds to states strongly localized in AA stacking regions of the moiré. Recently Lopes Dos Santos *et al.*[23] extended their treatment based on the continuum model to smaller angles and confirmed the localization of the states in the AA regions of the moiré pattern.

V. CONFINEMENT IN AA REGIONS

It is interesting to look at the band structures of bilayers with small angles—small enough to have Van Hove singularities at the limit of the linear variation (Fig. 4). The (19,20) bilayer is at the edge of the linear regime: The band structure still shows a linear dispersion and Van Hove singularities. For the (31,32) bilayer, bands are flat and the velocity is equal to zero[31] but in the case of the (45,46) bilayer, the peak at E_D is split in two and the velocity at the Dirac point increases again and is equal to ∼20% of the graphene velocity. This is coherent with the increase of velocity between magic angles found by Bistritzer and MacDonald[29] (Sec. VI).

It is important to notice that near the Dirac point one observes the existence of two bands that disperse linearly. These bands have a twofold degeneracy (Dirac cones from the two layers). The 4 bands contribute to the central peak of the total density of states. The weight of the eigenstates close to the Dirac energy is strong in the AA zone as shown by diagonalization.[31,35]

The analysis of the density of states shows that a specific regime occurs for very small angles, typically $\theta \leqslant 1^\circ$. The total DOS [Fig. 5(a)] contains sharp peaks at energies different from the Dirac energy. Figures 5(b) and 5(c) show the local DOS at the center of an AA stacked zone for decreasing θ, and Fig. 5(d) the local DOS at the center of an AB stacked zone.

For so small rotation angles, the moiré pattern presents well-defined regions of AA and AB stacking. In the center

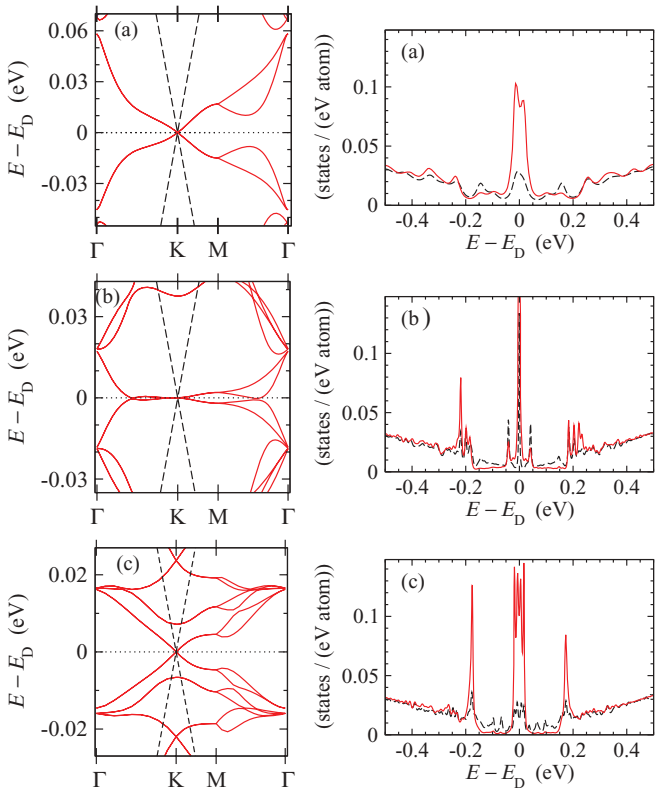

FIG. 4. (Color online) Band structures and DOS for bilayers with rotation angles that lead to Van Hove singularities close to the limit of the linear variation. (a) (19,20), $\theta = 1.67^\circ$; (b) (31,32), $\theta = 1.05^\circ$; (c) (45,46), $\theta = 0.73^\circ$. Left: Dispersion of monolayer graphene is shown in black dashed line for comparison. Right: (Red line) Local DOS at the center of AA zone, (black dashed line) total DOS.

of these regions, the local DOS follows the AA or AB DOS [dotted lines in Figs. 5(b), 5(c), and 5(d)], except for energies close to the Dirac energy. Indeed according to Fig. 5 peaks appear in an energy window defined by the mean interplane interaction γ_t. DOS in intermediate regions (not shown) are very similar to DOS in AB regions and do not show a large peak.

These results are consistent with confinement effect that can explain the discrete character of the spectrum in the $[-\gamma_t, +\gamma_t]$ range. Indeed, in large moiré patterns, AA regions seem isolated by AB and intermediate regions. From Fig. 5(d), we can say that confinement in AB regions is much less efficient than in AA regions. In a nanostructure, confinement results in a peak in the DOS whose position depends on the size of the nanostructure. Here the size of the AA region is inversely proportional to the rotation angle θ. In Fig. 6 we plot the energy of the first peak away from the Dirac energy as a function of θ. As expected this energy decreases when the size of the AA region increases, which is when the angle θ decreases.

In the energy range $[-\gamma_t, +\gamma_t]$, the symmetry of the wave function is different in an AA or AB bilayer [Fig. 7; see also the DOS in Fig. 10(b)]. Because of the different symmetry of the wave functions, matching is difficult which could explain that the AA stacked region is isolated. We note also that in this energy range the coupling between electrons and holes which have opposite velocities could favor localization. On

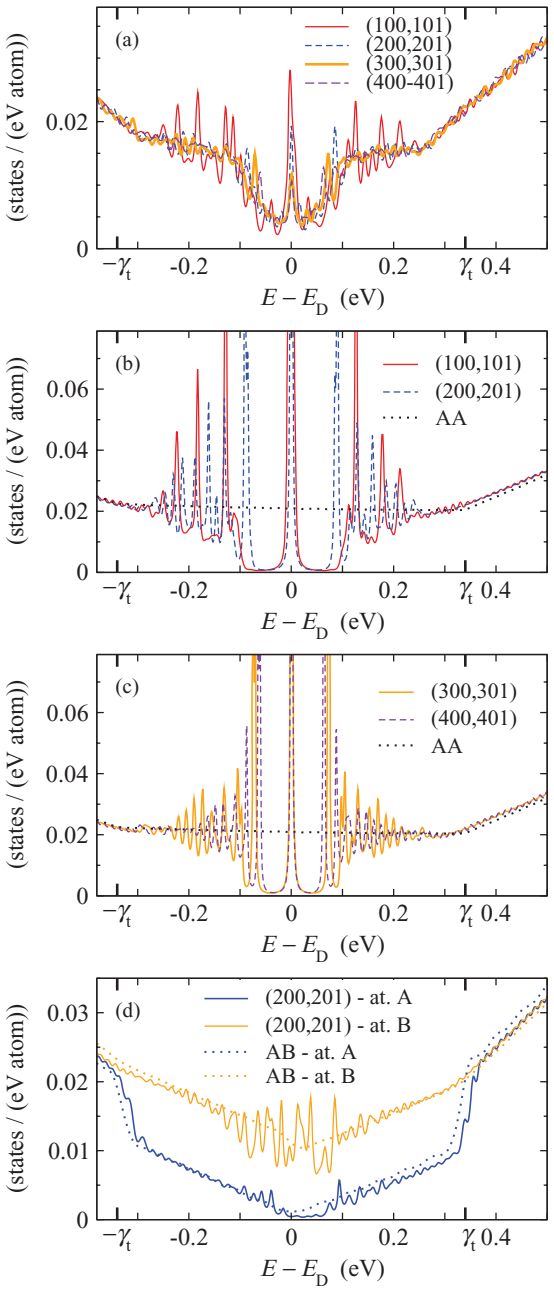

FIG. 5. (Color online) TB DOS in bilayers. (a) Total DOS. Local DOS: (b), (c) On atom at the center of an AA zone, (d) on atom at the center of an AB zone (at. A: with an atom directly on top or below; at. B: without an atom on top or below). (n,m) Bilayers: Values (100,101) $\theta = 0.33°$, (200,201) $\theta = 0.16°$, (300,301) $\theta = 0.11°$, (400,401) $\theta = 0.08°$.

the contrary out of the energy range $[-\gamma_t, +\gamma_t]$, the mixing between the hole states of one plane and the electron states of the other plane is weak. Indeed the coupling occurs between electron states of one plane and hole states of the other plane that have the same wave vector but have a difference in energy that is much larger than γ_t. Therefore outside of the energy range $[-\gamma_t, +\gamma_t]$ the mixing of states of the two planes occurs separately between the electron states of the two planes and between the hole states of the two planes. We suggest that this

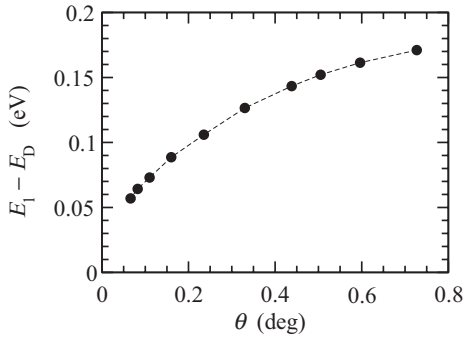

FIG. 6. Variation of the energy of the first peak (E_1) away from the Dirac point of the local DOS at the center of AA region as a function of θ.

absence of mixing between electrons and holes which have opposite velocities suppresses the localization.

VI. MAGIC ANGLES

As discussed previously, at very small angles, the velocity of rotated bilayers is no longer monotonic but shows minima and maxima (Fig. 8). Minima correspond to a flat band with zero velocity at the Dirac energy. Bistritzer and MacDonald in Ref. 29 found that the velocity is equal to zero for special magic angles θ_n. The values in degrees are $\theta_1 = 1.05, \theta_2 = 0.5$, $\theta_3 = 0.35$, $\theta_4 = 0.24$, $\theta_5 = 0.2$. We note that this series is simply given by $\theta_n = 1.05/n$. In the present calculations we recover by a full tight-binding calculation the first two angles $n = 1$ and $n = 2$ (see Fig. 8) which are given by $\theta_n = 1.13/n$ in good accordance with the more simplified model[36] of Ref. 29.

Below we propose a simple heuristic argument which relates these magic angles to quantization conditions. At these magic angles the bands become flat which means that the states of the different AA zones are decoupled and thus confined in the AA zones. In the following, we use a hard-wall model to describe the confinement effect. The confinement condition is typically

$$kd + 2\Phi = 2n\pi, \tag{3}$$

where k is the wave vector counted from the K point of the Dirac wave in the AA zone, $\frac{d}{2}$ is the typical size of the AA zone, and Φ is the phase accumulated at the reflection at the boundary of the AA zone. We assume that this phase can be integrated in an efficient size of the AA zone so that the

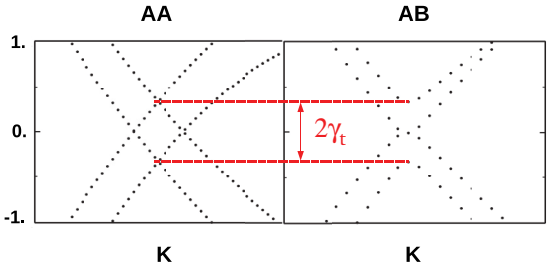

FIG. 7. (Color online) Band structure of an AA and an AB stacked bilayer in the vicinity of the Dirac energy.

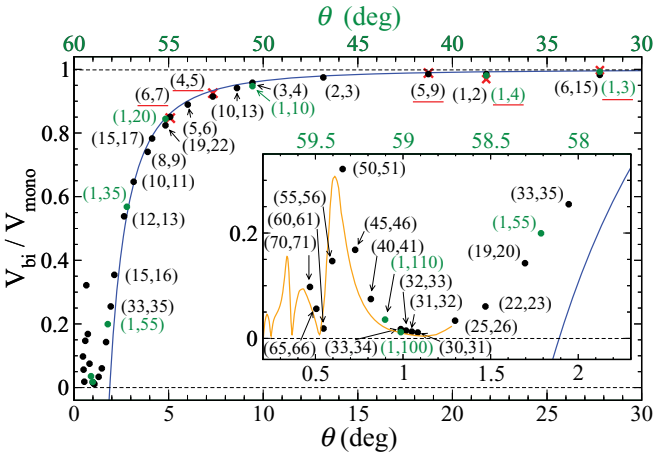

FIG. 8. (Color online) Velocity of a bilayer divided by the velocity of a monolayer, at the Dirac point, as a function of θ. The insert shows a zoom on very small angles and on angles close to 60°. Black/green point: TB calculation, red cross: *ab initio* calculation, blue line: law proposed by Lopes dos Santos *et al.* (Ref. 22), orange line: model proposed by Bistritzer and MacDonald (Ref. 29) for very small angles. The latter line is rescaled to obtain a first minimum of the velocity at 1.13° as in TB calculations (see text). *Ab initio* calculations and most of the TB calculations for $\theta > 1.05°$ are from Ref. 31.

quantization condition finally gives

$$xkD = 2n\pi, \tag{4}$$

where D is the period of the moiré and x is a numerical coefficient of the order of 1 such that $xD/2$ is the effective size of the AA zone. This expression can be cast in terms of the parameters of the present study. Indeed the period D of the moiré expressed in nanometers and the angle θ of the rotation expressed in degrees are related by $D(\text{nm}) = \frac{14}{\theta\ (\text{deg})}$ for small angles. In addition, we have the relation $\hbar v_F k = \gamma_t$ between the parameter γ_t and the wave vector k at the Dirac energy in the AA zone. Then the quantization relation leads to

$$\frac{3.4x\gamma_t\ (\text{eV})}{n} \sim \theta\ (\text{deg}). \tag{5}$$

For the present value of the parameter $\gamma_t = 0.34$ eV and with a reasonable value of the parameter $x \sim 0.95$ this relation leads exactly to the magic angles $\theta\ (\text{deg}) = 1.13/n$ found here. This value is close to the series $1.05/n$ found in Ref. 29.

Why the simple hard-wall argument discussed here can describe the magic angles series is not obvious. Indeed Bistritzer and MacDonald[29] used an interplane interaction Hamiltonian with a sinusoidal variation in space. For free electrons a sinusoidal interaction potential would probably not lead to the localization with hard-wall conditions. Yet as discussed above, the localization in the energy range $[-\gamma_t, +\gamma_t]$ that is found in this work suggest that the spinor character of the electronic wave function in graphene leads to more complex localization phenomena.

VII. CONCLUSION

Thanks to the tight-binding scheme that we developed, we studied the electronic structure of rotated bilayers in the case of very small rotation angles, which is beyond what was recently proposed. We showed that states are confined in regions of well-defined AA stacking and as a consequence that the LDOS shows discrete peaks not only at the Dirac energy but in the $[-\gamma_t, +\gamma_t]$ range with γ_t the mean interlayer hopping integral. Very large moiré patterns (corresponding to angles close to 1°) have already been observed experimentally. This system could then offer the possibility to study the physics of a regular array of weakly interacting dots. To conclude we note that the rotated bilayers of graphene present analogies with quasicrystals and approximant crystals that have also large unit cells and tend to confine electrons (Ref. 37 and references within). In the context of quasicrystals this localization by large unit cells leads to unique transport properties.[38,39] This suggests that rotated graphene bilayers with large unit cells could have original transport properties.

ACKNOWLEDGMENTS

The authors wish to thank P. Mallet and J.-Y. Veuillen for fruitful discussions. The computations have been performed at the Service Informatique Recherche (SIR), Université de Cergy-Pontoise, and on the CIMENT/PHYNUM project calculation center. We thank Y. Costes and David Domergue, Université de Cergy-Pontoise, and Dan Calugaru, Institut Néel, for computing assistance. We acknowledge financial support from RTRA (DISPOGRAPH project) and the French National Agency (ANR P3N/NANOSIM-GRAPHENE project).

APPENDIX: TIGHT-BINDING SCHEME FOR BILAYERS

In this Appendix we present in details the tight-binding (TB) scheme that we have used in our previous work[31] and in the present results. It reproduces the *ab initio* calculations of the electronic states for energies within ±2 eV of E_D whatever the rotation angle is (Figs. 9 and 10 and Ref. 31). Here E_D is set to zero.

Only p_z orbitals are taken into account since we are interested in what happens at the Fermi level. Since the planes are rotated, neighbors are not on top of each other (as is the case in the Bernal AB stacking). Interlayer interactions are then not restricted to $pp\sigma$ terms but some $pp\pi$ terms have also to be introduced. The Hamiltonian has the form

$$H = \sum_i \epsilon_i\, |i\rangle\langle i| + \sum_{\langle i,j\rangle} t_{ij}\, |i\rangle\langle j|, \tag{A1}$$

where $|i\rangle$ is the p_z orbital located at $\vec{r}_i$, and $\langle i,j\rangle$ is the sum on index i and j with $i \neq j$. The coupling matrix element, t_{ij}, between two p_z orbitals located at $\vec{r}_i$ and $\vec{r}_j$ is[40]

$$t_{ij} = n^2 V_{pp\sigma}(r_{ij}) + (1-n^2) V_{pp\pi}(r_{ij}), \tag{A2}$$

where n is the direction cosine of $\vec{r}_{ij} = \vec{r}_j - \vec{r}_i$ along (Oz) axis and r_{ij} the distance r_{ij} between the orbitals,

$$n = \frac{z_{ij}}{r_{ij}} \quad \text{and} \quad r_{ij} = ||\vec{r}_{ij}||. \tag{A3}$$

z_{ij} is the coordinate of $\vec{r}_{ij}$ along (Oz). It is either equal to zero or to a constant because the two graphene layers have been kept flat in our model.[41] We use the same following dependance on

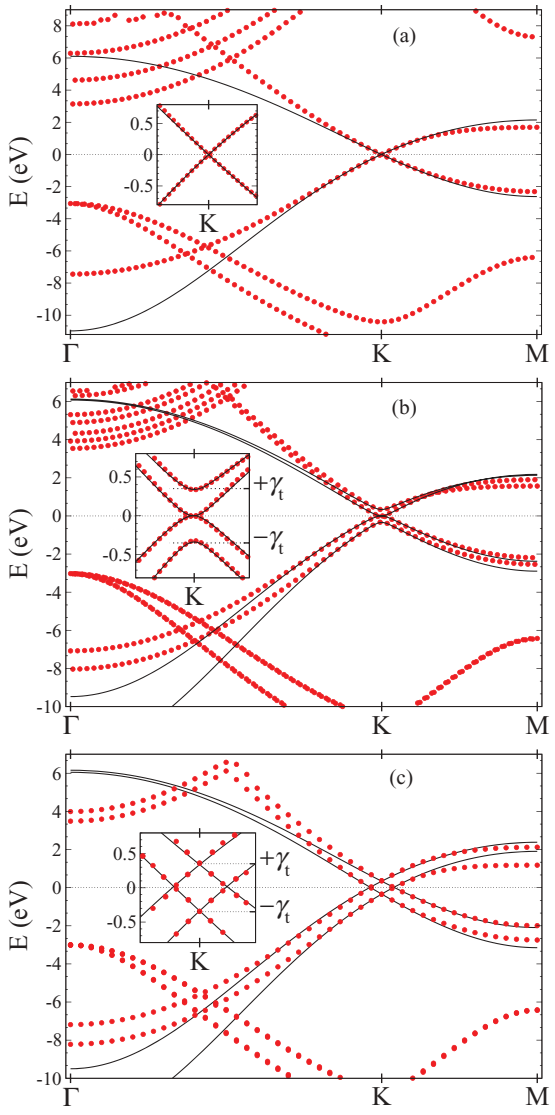

FIG. 9. (Color online) Band structure $E(\vec{k})$ calculated from *ab initio* VASP and TB: (a) graphene, (b) AB bilayer, (c) AA bilayer. $\gamma_t = 0.34$ eV.

distance of the Slater and Koster parameters:

$$V_{pp\pi}(r_{ij}) = -\gamma_0\, e^{q_\pi(1-r_{ij}/a)}\, F_c(r_{ij}), \tag{A4}$$

$$V_{pp\sigma}(r_{ij}) = \gamma_1\, e^{q_\sigma(1-r_{ij}/a_1)}\, F_c(r_{ij}), \tag{A5}$$

where a is the nearest-neighbor distance within a layer, $a = 1.418$ Å, and a_1 is the interlayer distance, $a_1 = 3.349$ Å. First-neighbors interaction in a plane is taken equal to the commonly used value, $\gamma_0 = 2.7$ eV.[2] Second-neighbors interaction γ_0' in a plane is set[2] to $0.1 \times \gamma_0$ which fixes the value of the ratio q_π/a in Eq. (A4). The interlayer coupling between two p_z orbitals in the π configuration is γ_1. γ_1 is fixed to obtain a good fit with *ab initio* calculation around Dirac energy in AA stacking and AB Bernal stacking and then to get $\gamma_t = 0.34$ eV (Figs. 7, 9, and 10) which results in $\gamma_1 = 0.48$ eV. We chose the same coefficient of the exponential decay for $V_{pp\pi}$

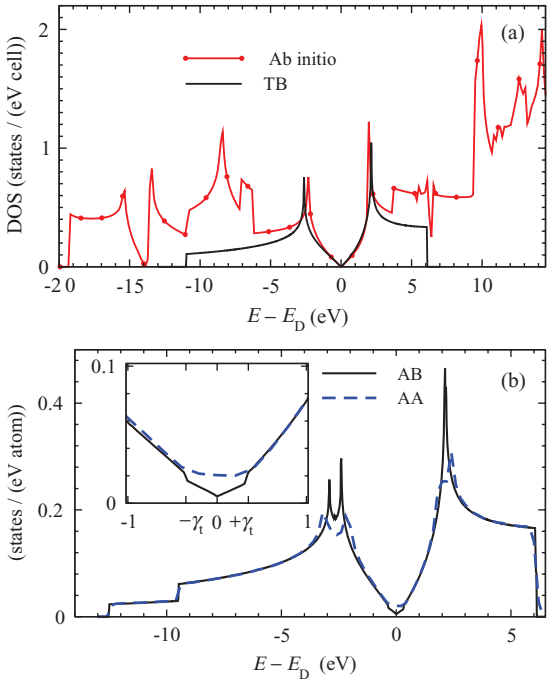

FIG. 10. (Color online) Density of states. (a) *Ab initio* [linear muffin tin orbitals (Ref. 42)] and TB total DOS in graphene. (b) TB total DOS in AB (Bernal) and AA bilayers. (Inset: Total DOS around the $E_D = 0$. $\gamma_t = 0.34$ eV.)

and $V_{pp\sigma}$,

$$\frac{q_\sigma}{a_1} = \frac{q_\pi}{a} = \frac{\ln(\gamma_0'/\gamma_0)}{a - a_0} = 2.218\ \text{Å}^{-1}, \tag{A6}$$

with $a_0 = 2.456$ Å the distance between second neighbors in a plane. Intralayer and interlayer coupling terms $t(r_{ij})$ calculated with these parameters are shown in Fig. 11. In (A4) and (A5), a smooth cutoff function is introduced,[43]

$$F_c(r) = (1 + e^{(r-r_c)/l_c})^{-1}, \tag{A7}$$

with r_c the cutoff distance and $l_c = 0.5$ a.u. $= 0.265$Å.[43] For $r \ll r_c$, $F_c(r) \simeq 1$; and for $r \gg r_c$, $F_c(r) \simeq 0$. All results presented in this article are calculated with $r_c = 2.5a_0 = 6.14$ Å.

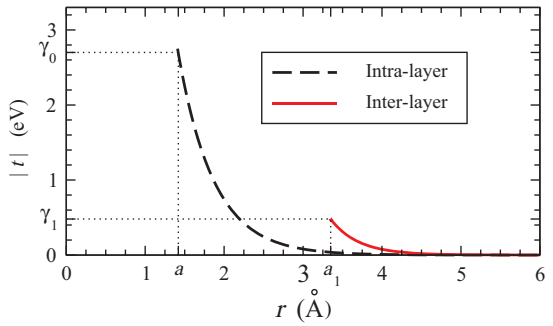

FIG. 11. (Color online) Coupling term t between two p_z orbitals versus the distance r: (full line) in two layers (interlayer coupling); (dashed line) in the same layer (intralayer coupling). Here, the smooth cutoff function F_c is not taken into account [i.e., large r_c value in (A7)].

We have checked that the results are independent of r_c for $r_c > 4.9$ Å.

All p_z orbitals have the same on-site energy ϵ_i [Eq. (A1)]. ϵ_i is set to -0.78 eV so that the energy E_D of the Dirac point is equal to zero in monolayer graphene. ϵ_i is not zero because the intralayer coupling between atoms beyond first neighbors breaks the electron/hole symmetry and then shifts E_D.

*guy.trambly@u-cergy.fr
†didier.mayou@grenoble.cnrs.fr
‡laurence.magaud@grenoble.cnrs.fr

[1] P. R. Wallace, Phys. Rev. **71**, 622 (1947).
[2] A. H. Castro Neto, F. Guinea, N. M. R. Peres, K. S. Novoselov, and A. K. Geim, Rev. Mod. Phys. **81**, 109 (2009).
[3] S. Latil and L. Henrard, Phys. Rev. Lett. **97**, 036803 (2006).
[4] F. Zhang, B. Sahu, H. Min, and A. H. MacDonald, Phys. Rev. B **82**, 035409 (2010).
[5] F. Varchon, P. Mallet, J.-Y. Veuillen, and L. Magaud, Phys. Rev. B **77**, 235412 (2008).
[6] T. Ohta, A. Bostwick, T. Seyller, K. Horn, and E. Rotenberg, Science **313**, 951 (2006).
[7] C. Coletti, C. Riedl, D. S. Lee, B. Krauss, L. Patthey, K. von Klitzing, J. H. Smet, and U. Starke, Phys. Rev. **81**, 235401 (2010).
[8] I. Brihuega, P. Mallet, C. Bena, S. Bose, C. Michaelis, L. Vitali, F. Varchon, L. Magaud, K. Kern, and J. Y. Veuillen, Phys. Rev. Lett. **101**, 206802 (2008).
[9] J. Hass, R. Feng, T. Li, X. Li, Z. Zong, W. A. de Heer, P. N. First, E. H. Conrad, C. A. Jeffrey, and C. Berger, Appl. Phys. Lett. **89**, 143106 (2006).
[10] J. Hass, W. A. de Heer, and E. H. Conrad, J. Phys.: Condens. Matter **20**, 323202 (2008).
[11] K. V. Emtsev, F. Speck, Th. Seyller, L. Ley, and J. D. Riley, Phys. Rev. B **77**, 155303 (2008).
[12] M. Sprinkle, D. Siegel, Y. Hu, J. Hicks, A. Tejeda, A. Taleb-Ibrahimi, P. Le Fèvre, F. Bertran, S. Vizzini, H. Enriquez, S. Chiang, P. Soukiassian, C. Berger, W. A. de Heer, A. Lanzara, and E. H. Conrad, Phys. Rev. Lett. **103**, 226803 (2009).
[13] J. Hicks *et al.*, Phys. Rev. B **83**, 205403 (2011).
[14] J. Hass, F. Varchon, J. E. Millan-Otoya, M. Sprinkle, N. Sharma, W. A. de Heer, C. Berger, P. N. First, L. Magaud, and E. H. Conrad, Phys. Rev. Lett. **100**, 125504 (2008).
[15] A. Luican, G. Li, A. Reina, J. Kong, R. R. Nair, K. S. Novoselov, A. K. Geim, and E. Y. Andrei, Phys. Rev. Lett. **106**, 126802 (2011).
[16] G. Li, A. Luican, L. M. B. Lopes dos Santos, A. H. Castro Neto, A. Reina, J. Kong, and E. Y. Andrei, Nat. Phys. **6**, 109 (2010).
[17] D. L. Miller, K. D. Kubista, G. M. Rutter, M. Ruan, W. A. de Heer, P. N. First, and J. A. Stroscio, Science **324**, 924 (2009).
[18] C. Berger, Z. M. Song, X. B. Li, X. S. Wu, N. Brown, C. Naud, D. Mayou, T. B. Li, J. Hass, A. N. Marchenkov, E. H. Conrad, P. N. First, and W. A. de Heer, Science **312**, 1191 (2006).
[19] M. L. Sadowski, G. Martinez, M. Potemski, C. Berger, and W. A. de Heer, Phys. Rev. Lett. **97**, 266405 (2006).
[20] F. Varchon, P. Mallet, L. Magaud, and J.-Y. Veuillen, Phys. Rev. B **77**, 165415 (2008).
[21] Z. Y. Rong and P. Kuiper, Phys. Rev. B **48**, 17427 (1993).
[22] J. M. B. Lopes dos Santos, N. M. R. Peres, and A. H. Castro Neto, Phys. Rev. Lett. **99**, 256802 (2007).
[23] J. M. B. Lopes dos Santos, N. M. R. Peres, and A. H. Castro Neto, arXiv:1202.1088.
[24] S. Latil, V. Meunier, and L. Henrard, Phys. Rev. B **76**, 201402(R) (2007).
[25] S. Shallcross, S. Sharma, and O. A. Pankratov, Phys. Rev. Lett. **101**, 056803 (2008).
[26] E. J. Mele, Phys. Rev. B **81**, 161405(R) (2010).
[27] E. J. Mele, Phys. Rev. B **84**, 235439 (2011).
[28] E. Suarez Morell, J. D. Correa, P. Vargas, M. Pacheco, and Z. Barticevic, Phys. Rev. B **82**, 121407(R) (2010).
[29] R. Bistritzer and A. H. MacDonald, Proc. Natl. Acad. Sci. USA **108**, 12233 (2011).
[30] R. Bistritzer and A. H. MacDonald, Phys. Rev. B **81**, 245412 (2010).
[31] G. Trambly de Laissardière, D. Mayou, and L. Magaud, Nano Lett. **10**, 804 (2010).
[32] I. Brihuega, P. Mallet, H. González-Herrero, G. Trambly de Laissardière, M. M. Ugeda, L. Magaud, J. M. Gómez-Rodríguez, F. Ynduráin, and J.-Y. Veuillen, arXiv:1209.0991.
[33] J. M. Campanera, G. Savini, I. Suarez-Martinez, and M. I. Heggie, Phys. Rev. B **75**, 235449 (2007).
[34] These calculations where performed with VASP with LDA which gives a better description of the interlayer distance.
[35] Let us note that other bands contribute also to the central peak of the density of states but do not give linear dispersion close to the Dirac points.
[36] In Fig. 8, the velocity (orange line) is plotted as a function of the angle θ and not α as in Ref. 29. For small angles, $\alpha = C/\theta$, where $C = \gamma_t/(\hbar V_{\text{mono}} K_D)$. In Ref. 29, parameters are deduced from experiment and lead to $C = 0.621$. We use a different TB scheme, fitted on *ab initio* calculations that underestimate velocity value. Therefore to compare our results with those in Ref. 29, we use $C = 0.67$ to obtain the same angle value for the first magic angle. This last C value is used to plot the orange variation.
[37] C. Berger, E. Belin, and D. Mayou, Annale de Chimie-Sciences des Materiaux **18**, 485 (1993).
[38] F. Triozon, Julien Vidal, R. Mosseri, and Didier Mayou, Phys. Rev. B **65**, 220202 (2002).
[39] G. Trambly de Laissardière, J.-P. Julien, and D. Mayou, Phys. Rev. Lett. **97**, 026601 (2006).
[40] J. C. Slater and G. F. Koster, Phys. Rev. **94**, 1498 (1954).
[41] The atomic positions of the (6,7) bilayer have been fully relaxed using VASP and the LDA functional without any noticeable effect either on the geometry—no buckling—or on the electronic structure.
[42] O. K. Andersen, Phys. Rev. B **12**, 3060 (1975).
[43] M. J. Mehl and D. A. Papaconstantopoulos, Phys. Rev. B **54**, 4519 (1996).